Light-Induced Structural Changes of LOV Domain-Containing Polypeptides from *Arabidopsis* Phototropin 1 and 2 Studied by Small-Angle X-ray Scattering†

Masayoshi Nakasako,*,‡,§ Tatsuya Iwata,||,⊥ Daisuke Matsuoka,|| and Satoru Tokutomi*,||

Department of Physics, Faculty of Science and Technology, Keio University, 3-14-1, Hiyoshi, Kohoku-ku, Kanagawa 223-8522, Japan, The RIKEN Harima Institute/SPring-8, 1-1-1 Kouto, Mikazuki, Sayo, Hyogo 679-5148, Japan, The Research Institute for Advanced Science and Technology, Osaka Prefecture University, 1-1 Gakuen-cho, Sakai, Osaka 599-8531, Japan, and Department of Material Science and Engineering, Nagoya Institute of Technology, Showa-ku, Nagoya 466-8555, Japan

Received July 9, 2004; Revised Manuscript Received September 21, 2004

ABSTRACT: Phototropin is a blue-light receptor of plants and comprises two light-receptive domains, LOV1 and LOV2, Ser/Thr kinase domain and one linker region connecting the LOV2 and the kinase domains. The LOV2 domain is thought to regulate predominantly the light-dependent autophosphorylation of the kinase domain, leading to cellular signaling cascades. In this study, we constructed recombinant LOV1, LOV2, and LOV2-linker polypeptides from phototropin 1 and phototropin 2 of *Arabidopsis thaliana* and studied their quaternary structures and light-dependent conformational changes by small-angle X-ray scattering. The molecular weights of the polypeptides determined from scattering intensities demonstrated the dimeric associations of LOV1 polypeptides of both isoforms. In contrast, while LOV2 and LOV2-linker polypeptides of phototropin 1 were homodimers, corresponding polypeptides of phototropin 2 existed as monomeric forms. Under blue-light irradiation, the LOV2-linker polypeptide of phototropin 1 displayed small but definite changes of the scattering profile. Through simulation of low-resolution molecular structures, the changes were likely explained as structural changes of the linker region and/or a movement of the region relative to the LOV2 domain. Light-induced profile changes were not observed in the $Cys^{512}Ala$ mutated LOV2-linker polypeptide of phototropin 1 losing the phototransformation capability. Thus, it was indicated that the photoreaction in the LOV2 domain probably caused the structural changes in the LOV2-linker polypeptide of phototropin 1. On the basis of the results, the interdomain interactions in phototropin are discussed.

Plants possess sensory systems composed of various types of proteins converting external physical or chemical stimuli, such as temperature, light, gravity, or chemical substrates, into biological signals to propagate to downstream components of cellular signal transduction systems. Visible light is an important stimulus that regulates precisely developmental and cell motility processes of plants. To sense light conditions, including intensity, quality, and direction, plants have acquired three major photoreceptors, phytochrome, cryptochrome, and phototropin (*1*). Phytochromes, mostly sensing red and far-red light (*2*), and cryptochromes, blue-light sensors (*3*), act as photoreceptors for seed germination, de-etiolation, and flowering through regulating gene expression.

Phototropin (*4*, *5*) is first identified as a photoreceptor for tropic responses (*6*) and is now known to regulate chloroplast relocations (*7*−*9*) and stomatal opening (*10*) to maximize the efficiency of photosynthesis. Blue light triggers the autophosphorylation of phot (*5*, *11*), resulting in the regulation of auxin transport (*12*) and the changes in Ca^{2+} concentration in cytoplasm (*13*, *14*). Most plants have two isoforms of phototropin named phot1[1] and phot2 (*4*). For instance, phot1 and phot2 of *Arabidopsis thaliana* regulate redundantly stomatal opening (*10*) through controlling the activity of a membrane-bound P-type H^+-ATPase (*15*). In addition, they share tropic responses and photoaccumulation of chloroplasts depending on the fluence rate of blue light (*8*). In contrast, only phot2 mediates the photoavoidance response in chloroplast relocation (*7*).

Phots comprise 900−1000 amino acid residues and two prosthetic flavin mononucleotide (FMN) molecules (*4*, *5*) (Figure 1A). The N-terminal half of phot folds into a pair of FMN-binding domains (ca. 110 residues). The domains are designated LOV1 and LOV2 (*16*) because their tertiary structures are highly homologous to those of the light, oxygen, and voltage (LOV)-sensing domains (*17*). The LOV domains are known to be a subset of the PER-ARNT-SIM

† This work was supported by grants in aid from MEXT Japan to M.N. (15076210) and S.T. (13139205). The SAXS experiments were carried out under the approval of the organizing committee of SPring-8 to M.N. (Proposals 2002B0152, 2003A0106, and 2003B-0141).

* To whom correspondence should be addressed. M.N.: phone, +81-45-566-1679; fax, +81-45-566-1672; e-mail, nakasako@phys.keio.ac.jp. S.T.: phone, +81-72-254-9841; fax, +81-72-254-9841; e-mail, toxan@riast.osakafu-u.ac.jp.

‡ Keio University.

§ The RIKEN Harima Institute/SPring-8.

|| Osaka Prefecture University.

⊥ Nagoya Institute of Technology.

[1] Abbreviations: phot1, phototropin 1; phot2, phototropin 2; FMN, flavin mononucleotide; NMR, nuclear magnetic resonance; SAXS, small-angle X-ray scattering; GST, glutathione *S*-transferase; PAGE, polyacrylamide gel electrophoresis; PBS, phosphate-buffered saline; R_g, radius of gyration.

10.1021/bi0485530 CCC: $27.50
Published on Web 11/05/2004

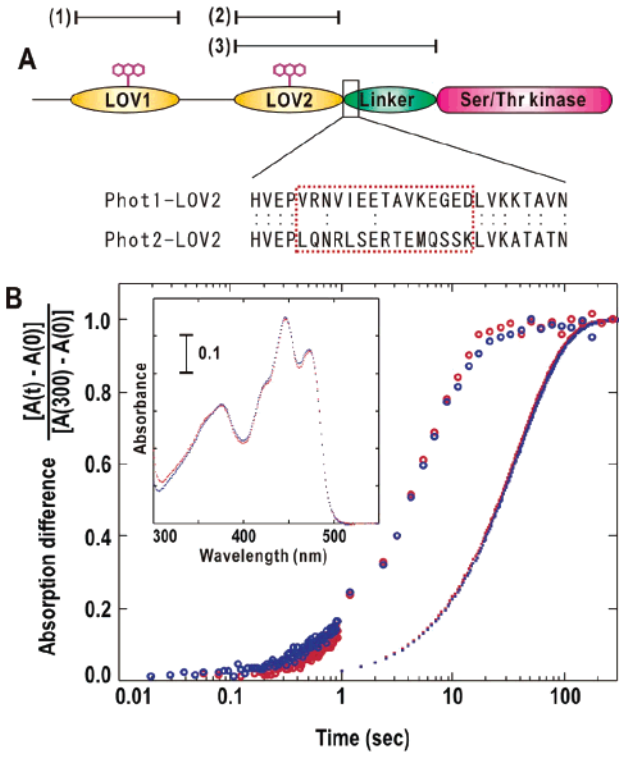

FIGURE 1: (A) Schematic illustration of the primary structure of phot1 and phot2 of *A. thaliana*. The regions of LOV polypeptides used in this study are shown with bars: (1) LOV1, (2) LOV2, and (3) LOV2-linker polypeptides. The box denotes the region within which the amino acid sequences are distinct between the two isoforms (see the Discussion). (B) Kinetics of dark reversion from the cysteinyl adduct state to the ground state monitored by absorption changes at 450 nm in phot1 LOV2 (blue dots), phot1 LOV2-linker (red dots), phot2 LOV2 (blue circles), and phot2 LOV2-linker (red circles) polypeptides. The absorption change at time t after a light flash $[A(t) - A(0)]$ is normalized by that at 300 s $[A(300) - A(0)]$ and plotted against logarithm of time. The inset shows the absorption spectra of phot1 LOV2-linker (red dots) and phot1 LOV2 (blue dots) in the dark.

(PAS) superfamily thought to act as protein−protein interaction modules in eukaryotic cellular signaling (*18*). The C-terminal half of phot forms a serine/threonine kinase domain (S/T-kinase) connected to the LOV2 domain by a linker region composed of ca. 85 residues (Figure 1A). Blue light-enhanced autophosphorylation of the kinase domain observed both *in vivo* (*11*) and *in vitro* (*6*) is thought to be a key process in the light-induced signal transduction mediated by phots.

Upon absorbing blue light, LOV domains undergo a unique photochemical reaction cycle by reversibly forming and breaking a covalent bond (*19*), cysteinyl adduct, between FMN and a highly conserved cysteine residue found in all LOV domains of phototropin-like proteins (*20*−*23*). Light-induced conformational changes in the protein moiety around the cofactor are very small as revealed in the crystal structure analyses of *Chlamydomonas* phot-LOV1 (*24*) and *Adiantum* phytochrome 3-LOV2 (*25*, *26*). Despite the small conformational changes in the photoreaction, the LOV domains are hypothesized to lead to the activation of the kinase domain through adduct formation (*27*). A rescue experiment for the phot-deficient *A. thaliana* mutant has revealed that the LOV2 domain regulates predominantly the kinase activity under the light condition (*28*). Recently, a nuclear magnetic resonance (NMR) study has revealed the light-dependent structural changes in a polypeptide comprising the LOV2 domain and a part of the linker region (*29*). These results suggest that light-induced changes in the interdomain interactions may be a key event for the activation of the kinase domain.

In this study, we constructed polypeptides containing either LOV domain of *A. thaliana* phot1 and phot2 (Figure 1A) and examined their quaternary structures and light-induced conformational changes by small-angle X-ray scattering (SAXS) (*30*). We established the oligomeric state of the LOV polypeptides and which polypeptides exhibited light-induced changes in SAXS. This structural study may provide clues for understanding how the domains communicate with each other, and how the light-induced small conformational changes in LOV2 domain propagate to the kinase domain.

MATERIALS AND METHODS

Preparation of Recombinant LOV Polypeptides. Six wild-type polypeptides containing either the LOV1 or LOV2 domain of *A. thaliana* phot1 or phot2 were prepared by overexpression systems with *Escherichia coli*. The recombinant polypeptides are LOV2-linker polypeptides comprising the LOV2 domain and the linker region, LOV1 polypeptides, and LOV2 polypeptides from phot1 and corresponding three polypeptides from phot2 (Figure 1A and Table 1). All polypeptides included additional extensions of some amino acid residues at both the N- and C-terminal ends of the LOV core (104 amino acid residues) (Table 1).

Using the cDNA of *A. thaliana* phot1 and phot2 as templates, DNA fragments corresponding to the LOV polypeptides were amplified by the PCR method with oligonucleotide primers providing appropriate restriction sites. The amplified DNAs were isolated, digested, and cloned into pGEX4T1 bacterial expression vectors (Amersham Biosience) as fusion proteins with glutathione *S*-transferase (GST). A linker sequence (Gly-Ser-Pro-Glu-Phe) was inserted to connect the N-terminal end of a polypeptide and the C-terminal end of GST. In addition to the wild-type polypeptides, the Cys^{512}Ala mutant LOV2-linker polypeptide of phot1 was prepared for a reference experiment (see the Results). The mutation was introduced by using a Quick Change Site-directed Mutagenesis Kit (Amersham Bioscience) and was verified by DNA sequencing with a CEQ 200XL DNA Analysis System (Beckman Coulter). The mutant polypeptide completely lost the capability of formation of the cysteinyl adduct under blue-light irradiation (*20*).

JM109 strains of *E. coli* transformed by the expression vectors were grown at 310 K in L-broth containing 50 μg/mL ampicillin until the A_{600} had reached 0.3, and then incubated in the dark for a further 20 h at 293 K in the presence of 0.1 mM isopropyl β-D-thiogalactopyranoside. The following purification procedures were carried out at 273−277 K under dim red light. Harvested bacteria were lysed in phosphate-buffered saline containing 1 mM phenylmethanesulfonyl fluoride, and the supernatant was mixed with glutathione−Sepharose 4B (Amersham Bioscience). Fusion proteins were eluted with a solution containing 10 mM reduced glutathione, 50 mM Tris-HCl, 100 mM NaCl, and 1 mM EGTA (pH 7.5). GST tags were removed by thrombin digestion at the linker sequence. The cleaved LOV-polypeptide was purified further by gel chromatography with Sephacryl S-100 HR (Pharmacia) and a buffer solution

Table 1: Molecular Weights and Structural Parameters of the LOV Polypeptides

polypeptide (starting and ending residues)	M_w of the sequence	$I(0,0)^a$ (relative)	M_w (k) SAXS	oligomeric state	$R_g(0)$ (Å)^b	D_{max} (Å)^b	χ^2 of GASBOR models^c (DAMMIN)
phot1							
LOV1	17 135	12.8 ± 0.6	35 ± 2	dimer	23.5 ± 0.3	100 ± 3	1.83 (1.57)
(180G−329K)					23.1 ± 0.4	100 ± 3	
LOV2-linker	24 933	16.8 ± 0.9	46 ± 3	dimer	31.3 ± 0.3	122 ± 3	1.44 (1.37)
(449E−661K)		17.2 ± 0.9	47 ± 3		32.6 ± 0.3	135 ± 4	1.43 (1.37)
LOV2-linker	24 901	16.8 ± 0.7	46 ± 2	dimer	31.0 ± 0.3	122 ± 3	
Cys^{512}/Ala					31.2 ± 0.3	122 ± 3	
LOV2	15 621	11.3 ± 0.7	31 ± 2	dimer	20.7 ± 0.2	98 ± 3	2.45 (1.82)
(449E−578G)					20.8 ± 0.2	98 ± 3	
phot2							
LOV1	17 238	12.3 ± 0.6	33 ± 2	dimer	22.2 ± 0.3	94 ± 3	1.65 (1.46)
(117F−265K)					22.6 ± 0.3	94 ± 3	
LOV2-linker	25 046	8.8 ± 0.7	24 ± 2	monomer	24.3 ± 0.3	107 ± 3	1.50 (1.37)
(363D−575H)					25.0 ± 0.4	110 ± 3	
LOV2	16 699	5.7 ± 0.9	16 ± 3	monomer	20.2 ± 0.2	72 ± 2	1.44 (1.40)
(363D−500Q)					20.1 ± 0.3	72 ± 2	

[a] $I(0,0)$ values of BSA and lysozyme were 24.3 ± 0.5 and 5.6 ± 0.7, respectively. [b] The $R_g(0)$ and D_{max} values calculated from SAXS profiles in the dark and under blue-light irradiation are shown in the top and bottom rows, respectively. [c] The χ^2 values are calculated from the best-fit structures to the experimental SAXS profiles (see also Figure 2).

containing 100 mM NaCl, 25 mM Tris-HCl, and 1 mM Na_2-EDTA (pH 7.8). The eluted polypeptide solutions exhibited single bands upon Coomassie Brilliant Blue staining after SDS−polyacrylamide gel electrophoresis (PAGE). The molecular mass of either recombinant polypeptide and the purity of the sample were also examined by time-of-flight mass spectrometry with an AXIMA-QIT instrument (Shimadzu). The purified enzyme was concentrated by ultrafiltration.

Measurements of UV−Visible Absorption Spectra and Dark Reversions from a Cysteinyl Adduct State. Absorption spectra of the dark-adapted state and the kinetics during the thermal decay from the cysteinyl adduct state to the dark-adapted state of LOV2 polypeptides were measured at 293 K with a DynaSpect spectrophotometer (Hamamatsu Photonics). The decays were monitored every 300 ms after a light flash (duration of 350 μs) through a high-pass filter (L42, Toshiba). Absorption measurements of the other polypeptides were carried out using a U-3310 spectrophotometer (Hitachi). A photodiode illuminator is used for the accumulating cysteinyl adduct state. All polypeptide samples were concentrated to give a final absorbance of 0.1 at 450 nm in the dark-adapted state (Figure 1B).

SAXS Experiments. SAXS data were collected at the BL40B2 station of SPring-8 using an R-axis IV^{++} system as a detector (Rigaku). The X-ray wavelength was tuned to 1.000 Å, and the camera distance was set at 1050 mm. The temperatures of the samples were kept at 293 K. A sample cell with the thickness of 3.0 mm was used to measure optimally scattered X-rays. The windows of the cell were made of 0.01 mm thick quartz plates. The exposure time was 60 s for each measurement, and the current of an ionization chamber monitoring the intensity of the incident X-ray beam was integrated to normalize scattering intensities. To avoid systematic errors, sample and buffer solutions were measured alternately. No radiation damage of any sample was confirmed by the stabilities of SAXS profiles in five iterative exposures, slight changes in the absorption spectra, and the SDS−PAGE pattern of samples after X-ray exposures.

For each polypeptide, SAXS profiles were collected in the concentration range from 1 to 4 mg/mL with an increment of 0.5 or 1.0 mg/mL. A pair of profiles both in the dark and under blue-light irradiation was taken from the same sample by only turning off and on blue light supplied by a 1 kW projector and a filter sheet (λ_{max} = 480 nm, half-width = 40 nm; 4515C, Nakagawa Chemicals). When SAXS profiles were recorded under blue-light irradiation, the samples were preirradiated for 4 min before being exposed to X-rays to ensure the photostationary state with high population of the light-activated polypeptides. In every series of experiments, SAXS profiles of hen egg white lysozyme (M_w = 14 300, Sigma) or bovine serum albumin (M_w = 66 000, Sigma) were collected in the concentration range of 1.0−4.0 mg/mL as a reference for molecular weight determination.

Processing and Analyses of SAXS Data. IISGNAPR (*31*) was used for circular averaging of two-dimensionally recorded scattering patterns and background subtraction. Scattering profiles in the small-angle region were analyzed by Guinier's approximation for monodispersive systems (*32*): the scattering intensity $I(S,C)$, as a function of scattering vector S and protein concentration C, is expressed by the forward scattering intensity, $I(0,C)$, and the radius of gyration, $R_g(C)$, as

$$I(S,C) = I(0,C)\exp[-4\pi^2/3 \times R_g(C)^2S^2],\ S = 2\sin\theta/\lambda$$

where 2θ is the scattering angle and λ is the X-ray wavelength. $I(0,C)$ and $R_g(C)$ were alternatively obtained from the pair-distribution function [$P(r)$] calculated by using GNOM (*33*). In particular, when analyzing SAXS profiles with aggregation effects in the innermost scattering angles, the program could eliminate the effects by discarding the data points in the very small angle regions as carried out in SAXS studies on nucleocytoplasmic transport factors (*34*).

Under diluted conditions, $I(0,C)$ and $R_g(C)^2$ are expressed as

$$KC/I(0,C) = 1/M_w + 2A_2C + ...$$

$$R_g(C)^2 = R_g(0)^2 - B_{if}C + ...$$

where K is a constant, M_w is the molecular weight of the solute, A_2 is the second virial coefficient, and B_{if} is a

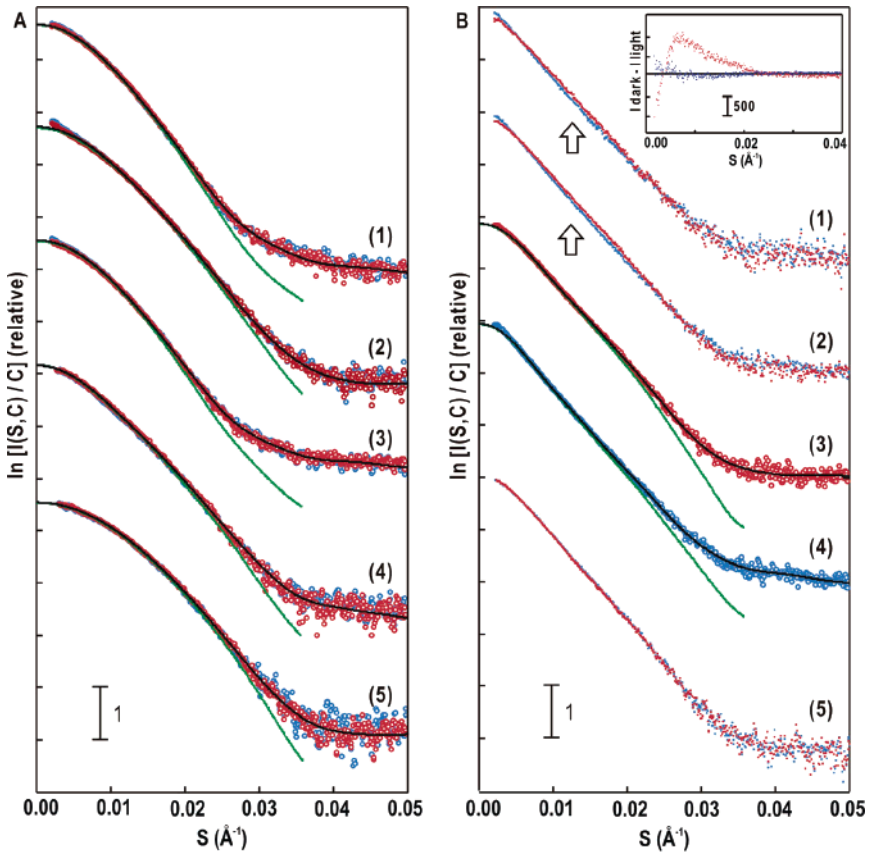

FIGURE 2: SAXS profiles of LOV polypeptides measured in the dark (red symbols) and under blue-light irradiation (blue symbols). The scattering intensities are plotted in semilogarithmic form and shifted appropriately along the ordinate for clarity. The black and green lines are profiles of structural models predicted by GASBOR (Figures 6 and 7) and DAMMIN, respectively. The χ^2 values of models are listed in Table 1: (A) phot1 LOV1 polypeptide (4 mg/mL solution) (1), phot1 LOV2 (4 mg/mL) (2), phot2 LOV1 (4 mg/mL) (3), phot2 LOV2-linker (3 mg/mL) (4), and phot2 LOV2 (2 mg/mL) (5) and (B) phot1 LOV2-linker polypeptide from 2 mg/mL (1) and 4 mg/mL (2) solutions. Two profiles in part 2 are shown separately in parts 3 and 4 to compare them with the calculated profiles of the predicted structures. Part 5 shows data for the Cys^{512}Ala mutant LOV2-linker polypeptide (4 mg/mL). Arrows denote the region where intensity changes are most prominent between the dark and light conditions. The inset shows the intensity differences between the dark and light conditions of the wild-type phot1 LOV2-linker (red dots) and those of the mutated polypeptides (blue dots). The difference profiles are calculated from the pairs in parts 2 and 5. In the wild-type phot1 LOV2-linker polypeptide, the difference at around $S = 0.008$ Å^{-1} is 5.5% of the scattering intensity in the dark.

parameter reflecting intersolute force potential. The sign of B_{if} is the same as that of A_2 (*32*). Assuming the partial specific volume of 0.74 cm^3/g for soluble proteins, the M_w of a protein is determined by using $I(0,C=0)$ of a reference protein with a known molecular weight.

Molecular structures of the polypeptides were predicted by applying the *ab initio* structure determination program DAMMIN (*35*) to scattering profiles weighted by S^{-4} to ensure Porod's law in $S < 0.035$ Å^{-1} and GASBOR (*36*) to those in $S < 0.05$ Å^{-1}. The programs minimized the discrepancy between the experimental $[I_{exp}(S)]$ and calculated $[I_{model}(S)]$ profiles by keeping a compactly interconnected configuration of dummy particles. Discrepancies are examined with the χ^2 values (*34*, *35*) defined as

$$\chi^2 = 1/(N-1)\sum_j \{[I_{exp}(S_j) - KI_{model}(S_j)]/\sigma(S_j)\}^2$$

where N is the number of experimental data points, K is a scaling factor, and $\sigma(S_j)$ is the statistical error of $I_{exp}(S_j)$ at the scattering vector S_j. In simulating the molecular structure of a dimeric polypeptide, we assumed 2-fold rotational symmetry. Because the *ab initio* analyses do not provide a unique solution for the three-dimensional structure, 10 independent calculations were carried out for each polypeptide. The predicted molecular structures having almost the same overall structures were aligned and averaged with SUPCOMB (*37*).

RESULTS

Dark Reversion Kinetics from the Cysteinyl Adduct State Monitored by UV−Visible Absorption. Figure 1B shows the dark reversion kinetics from the cysteinyl adduct state in LOV2 and LOV2-linker polypeptides. The half-life of the phot1 LOV2-linker polypeptide is 25.7 s, whereas that of the corresponding phot2 polypeptide is 3.9 s. The values are comparable to those of 29 s for phot1 LOV2 and 5 s for phot2 LOV2 polypeptides (*38*). Thus, the linker region has little influence on the lifetime of the cysteinyl adduct state of the LOV2 polypeptide of either isoform. Half-lives of the LOV1 polypeptides (data not shown) are also comparable to the reported values (*38*).

SAXS Profiles of the LOV Polypeptides. Figure 2 shows SAXS profiles of LOV polypeptides both in the dark and under blue-light irradiation. LOV1 polypeptides of both phot1 and phot2, LOV2-linker, and LOV2 polypeptides of phot2 exhibit monodispersive properties as indicated by the Guinier

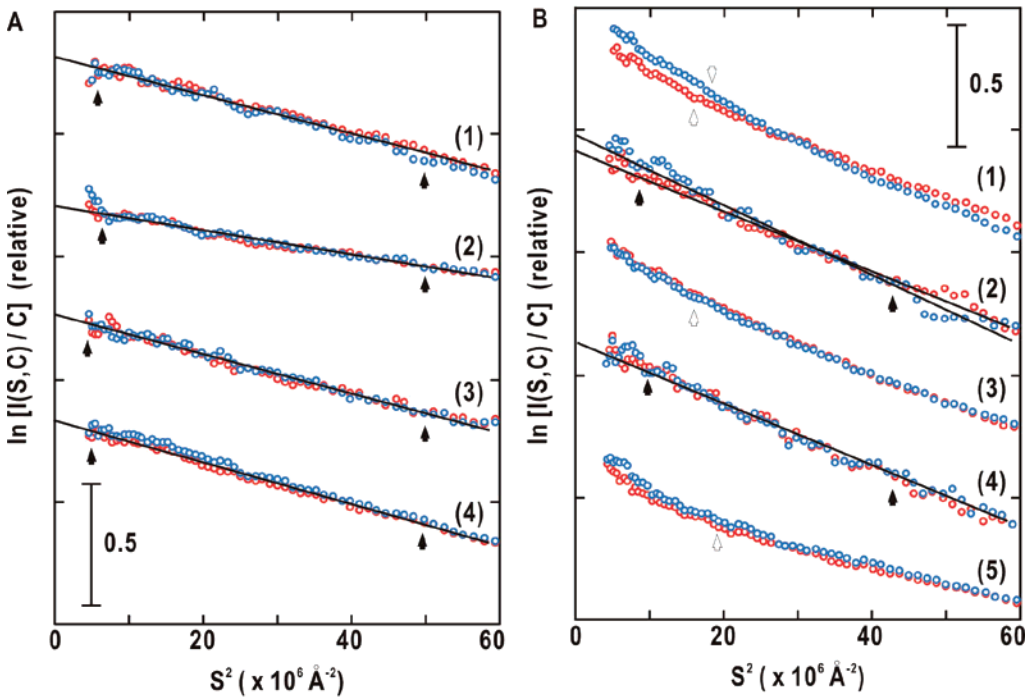

FIGURE 3: Guinier plots, logarithm of scattering intensities plotted against the square of the scattering vector, of seven LOV polypeptides in the dark (red symbols) and under blue-light irradiation (blue symbols): (A) phot2 LOV2-linker (2 mg/mL) (1), phot2 LOV2 (3 mg/mL) (2), phot2 LOV1 (2 mg/mL) (3), and phot1 LOV1 (3 mg/mL) (4) and (B) phot1 LOV2-linker (3 mg/mL) (1), phot1 LOV2-linker (1 mg/mL) (2), phot1 LOV2-linker with the $Cys^{512}Ala$ mutation (3 mg/mL) (3), phot1 LOV2-linker with the $Cys^{512}Ala$ mutation (1 mg/mL) (4), and phot1 LOV2 (3 mg/mL) (5). The regions used for the Guinier approximations are denoted by pairs of filled arrows. The high-angle edges of these regions satisfy the criteria for the approximation [$SR_g < (2\pi)^{-1}$]. The empty arrow in panel B denotes the low-angle border of data ($S = 0.004$ Å^{-1}) used for the GNOM analysis to calculate $I(0,C)$ and $R_g(C)$ values from the $P(r)$ functions. When the data points are included at $S < 0.004$ Å^{-1} in GNOM calculations, the profiles of the resultant $P(r)$ functions are unstable against small changes in the maximum dimensions given prior to the calculation. It should be noted that Guinier approximations applied for the data points at $S > 0.004$ Å^{-1} gave the structural parameters consistent with those from the GNOM analyses.

plots to be approximated by single regression lines (Figure 3A and Table 1). In wild-type and mutated phot1 LOV2-linker polypeptides, while the Guinier plots of profiles from 1 mg/mL solutions are approximated by single regression lines (2 and 4 in Figure 3B), aggregation effects are observed in the concentration range of 2−4 mg/mL (1 and 3 in Figure 3B). These suggest monodispersive properties of the two polypeptides under the diluted condition. Aggregation effects in phot1 LOV2 polypeptides (5 in Figure 3B) appear throughout the measured concentration range. Thus, $I(0,C)$ and $R_g(C)$ of the three polypeptides shown Figure 4 are estimated from $P(r)$ functions (Figure 5) calculated by applying GNOM to the profiles without the data points in $S < 0.004$ Å^{-1}.

Molecular models of each polypeptide predicted by GASBOR and DAMMIN are similar and give profiles consistent with the experimental ones as indicated by the small χ^2 values (Figure 2 and Table 1).

Oligomeric State of the LOV Polypeptides. Figures 4 presents the concentration-dependent variations of $C/I(0,C)$ and $R_g(C)^2$. $I(0,0)$ and $R_g(0)$ of polypeptides displaying monodispersive properties in their Guinier plots (Figure 3A) are determined by extrapolating the dependence to the infinitely diluted condition ($C = 0$) (Table 1). Those polypeptides with aggregation effects are estimated under the assumption that the effects are almost eliminated by the GNOM analyses.

The oligomeric state of a polypeptide is judged by comparing M_w calculated from the amino acid sequence and that estimated from $I(0,0)$ (Figure 4A,B and Table 1). LOV1 polypeptides of both phot1 and phot2 form dimers. In contrast, while LOV2 and LOV2-linker polypeptides of phot1 are dimers, corresponding polypeptides of phot2 are monomers. The $I(0,0)$ values of all polypeptides are almost independent of the dark or light conditions. Thus, no light-dependent dimer-to-monomer dissociation or monomer-to-dimer association occurs in the concentration range that was examined.

Except for the phot1 LOV2-linker polypeptide, the concentration dependences of $R_g(C)^2$ are almost the same between the dark and light conditions, indicating that the surface properties under blue-light irradiation are unchanged from those in the dark (Figure 4C,D and Table 1). The $R_g(0)^2$ values of the phot1 LOV2-linker polypeptides are distinct between the dark and light conditions, indicating the light-induced structural changes probably increase the size of the molecules. In addition, the positive gradient of R_g dependence under the light condition suggests more attractive intermolecular interaction than in the dark. Light-induced changes in surface properties may cause nonspecific aggregation of the phot1 LOV2-liner polypeptide (Figure 3B).

SAXS of phot2 LOV2 and LOV2-Linker Polypeptides. The M_w values of phot2 LOV2-linker and LOV2 polypeptides are consistent with those calculated from their primary sequences (Figure 4 and Table 1). The SAXS profile of the LOV2-linker polypeptide differs from that of the LOV2 polypeptide (Figure 2B). To date, the linker region has been believed to be a flexible loop connecting the LOV2 and

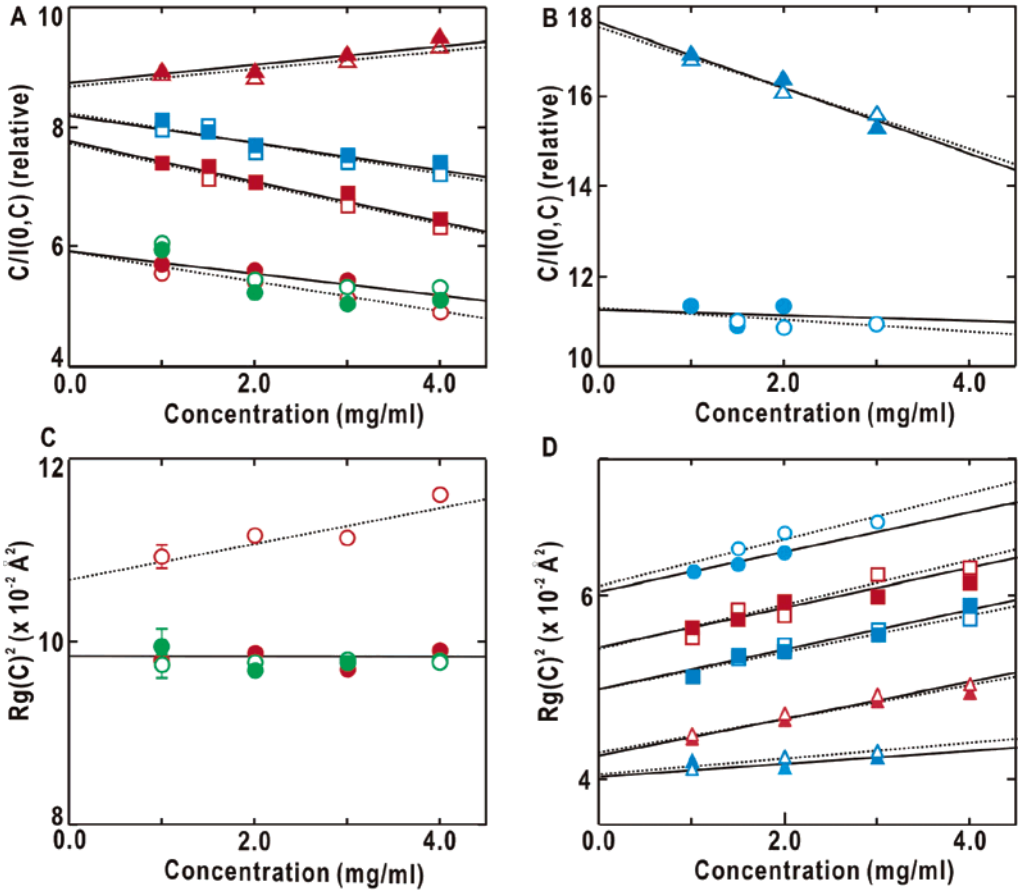

FIGURE 4: Concentration-dependent variations of $C/I(0,C)$ (A and B) and $R_g(C)^2$ (C and D). Data for phot1 polypeptides are colored red and those for phot2 polypeptides blue. Green symbols are used for the data of the Cys^{512}Ala mutant LOV2-linker polypeptide. Filled symbols represent the data in the dark and empty ones those under blue-light irradiation. Data from LOV1, LOV2, and LOV2-linker polypeptides are shown with squares, triangles, and circles, respectively.

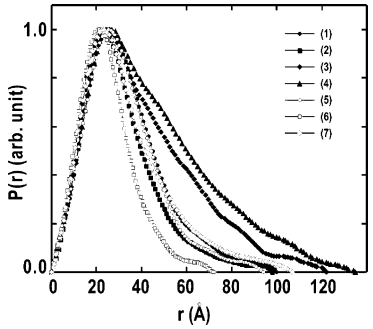

FIGURE 5: $P(r)$ functions of phot1 LOV1 (1), phot1 LOV2 (2), phot1 LOV2-linker (3), phot2 LOV1 (5), phot2 LOV2 (6), phot2 LOV2-linker in the dark (7), and phot1 LOV2-linker under blue-light irradiation (4).

kinase domains despite the lack of structural evidence. However, these results indicate that the linker region folds into a compact structure to contribute significantly to scattering intensities rather than a flexible and extended loop conformation. Thus, the phot2 LOV2-linker polypeptide is expected to be composed of the LOV2 domain and the linker "domain".

The SAXS profiles of the phot2 LOV2 polypeptide under blue-light irradiation are almost the same as those in the dark (Figures 2A). The results are consistent with those from the crystallographic studies on *Adiantum* phy3-LOV2, demonstrating only small conformational changes around FMN in the light-activated state (*26*). The molecular model of the LOV2 polypeptide is simulated as an anisotropic shape (Figure 6A) resembling the crystal structures of *Adiantum* phy3-LOV2 (*25*) and *Chlamydomonas* phot-LOV1 (*24*).

Under blue-light irradiation, SAXS profiles of the phot2 LOV2-linker polypeptide exhibit a very small decrease at around $S = 0.01$ Å^{-1} (data not shown); however, the magnitude is much smaller than that observed in the LOV2-linker polypeptide of phot1. The predicted molecular model of the polypeptide appears as an elongated shape (Figure 7A). The molecular model of the phot2 LOV2 polypeptide (Figure 6A) likely fits to the middle portion, and the lower portion probably corresponds to the linker domain.

SAXS of LOV1 Polypeptides. LOV1 polypeptides of both phot1 and phot2 exist as a dimer in solution (Table 1). They show no detectable changes in SAXS profiles and in the structural parameters between the dark and light conditions (Figure 2B and Table 1). These results are consistent with the crystal structure analyses of the *Chlamydomonas* phot-LOV1 domain, revealing little structural change under light-irradiation (*23*). The predicted molecular structure of the dimeric phot1-LOV1 polypeptide is likely approximated by two phot2-LOV2 models associating in an antiparallel orientation (Figure 6B). The molecular structure of the phot2-LOV1 polypeptide (Figure 6C) has a molecular shape and dimensions similar to those of phot1-LOV1 polypeptides (Figure 6B).

SAXS of phot1 LOV2 and LOV2-Linker Polypeptides in the Dark. LOV2 and LOV2-linker polypeptides of phot1 are

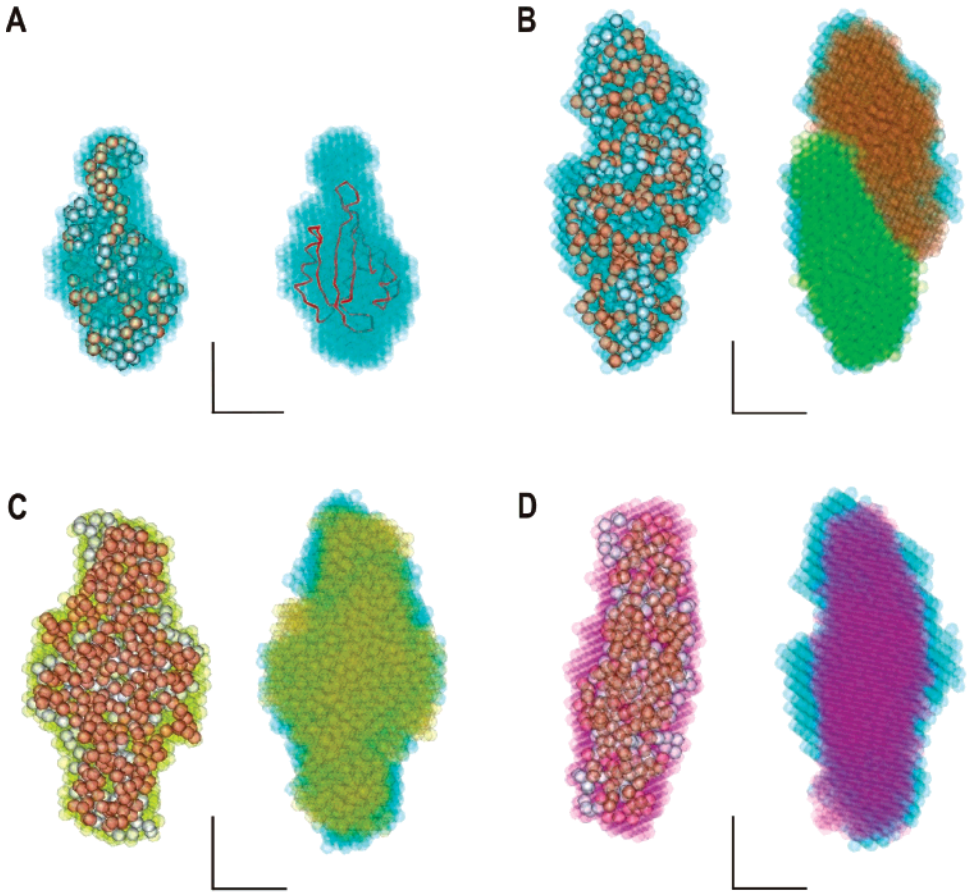

FIGURE 6: Molecular models of LOV polypeptides predicted by GASBOR. The χ^2 value of the structural model yielding the best fit to the experimental SAXS profile is given in Table 1. The molecular models are illustrated as assemblies of transparent spheres representing dummy scatterers used in the simulation. In the left part of each panel, the models yielding the best (white spheres) and the second best (brown) χ^2 values are superimposed on the average model calculated from the five best models (cyan spheres in panel A, yellow in panel C, and violet in panel D). The scale bar is 20 Å. (A) Molecular models of the phot2 LOV2 polypeptide. The red line in the right part represents the Cα trace of the phy3 LOV2 crystal structure manually fitted to the average structure. (B) Molecular models of the phot1 LOV1 polypeptide. The right part illustrates one possible approximation of the averaged model by an association of two models of the phot2 LOV2 polypeptide in panel A (spheres colored green or brown). (C) Molecular models of the phot2 LOV1 polypeptide. The average model (yellow) is compared with that of phot1 LOV1 (cyan) in the right part. (D) Molecular models of the phot1 LOV2 polypeptide. In the right part, the average model (purple) is superimposed on that of the dimeric phot1 LOV1 polypeptide (cyan) to overlap maximally. This figure was prepared with ASSA (*44*).

dimers in solution, in contrast to the corresponding polypeptides of phot2 (Figure 4 and Table 1). The linker region of the LOV2-linker polypeptide is also expected to fold into a compact structure as well as that of phot2. The predicted models of phot1 LOV2 (Figure 6D) have molecular dimensions comparable with those of LOV1 dimer models (Figure 6B,C), but their shapes differ slightly.

The molecular model of the dimeric LOV2-linker polypeptide is approximated as an elongated shape (Figure 7B) and is consistent with the characteristics of the computed $P(r)$ function, suggesting an extremely elongated shape (Figure 5). The molecular shape of the fragment may be approximated by two phot2 LOV2-linker models associating in an antiparallel orientation. Thus, the outer-edge portions of the molecular model probably correspond to the linker domains.

Blue-Light-Induced SAXS Changes of phot1 LOV2-Linker Polypeptide. The SAXS profiles of the phot1 LOV2-linker polypeptide under blue-light irradiation show small but definite changes from that in the dark (Figure 2B). The scattering intensities in an S between 0.003 and 0.005 Å^{-1} increase, while those in an S between 0.005 and 0.025 Å^{-1} decrease (inset of Figure 2B). The increase is partly interpreted as aggregation in the phototransformed state of fragments. Using the reciprocity between the scattering vector and distance of electron pairs in solute, the profile changes in $0.005 < S < 0.025$ Å^{-1} suggest structural changes on a scale of ca. 100 Å. The $R_g(0)$ and D_{max} values under light irradiation which are larger than in the dark (Figures 3B, 4C, and 5 and Table 1) indicate light-induced structural changes expand the size of the molecules. Figure 7C illustrates the predicted molecular structure of the LOV2-linker polypeptide under blue-light irradiation. The elongated shape found in the dark state is still retained; however, it significantly differs from that in the dark at the linker-domain regions.

The blue-light-induced SAXS changes are expected to be caused by the cysteinyl adduct formation in the LOV2 core. To confirm this, SAXS of the Cys^{512}Ala mutant phot1-LOV2A polypeptide was measured (Figures 2 and 3). The SAXS profile of the mutated polypeptide under blue-light irradiation is almost the same as that in the dark. The concentration dependences of $C/I(0,C)$ and $R_g(C)^2$ also resemble those of the wild type in the dark (Figures 4). Thus,

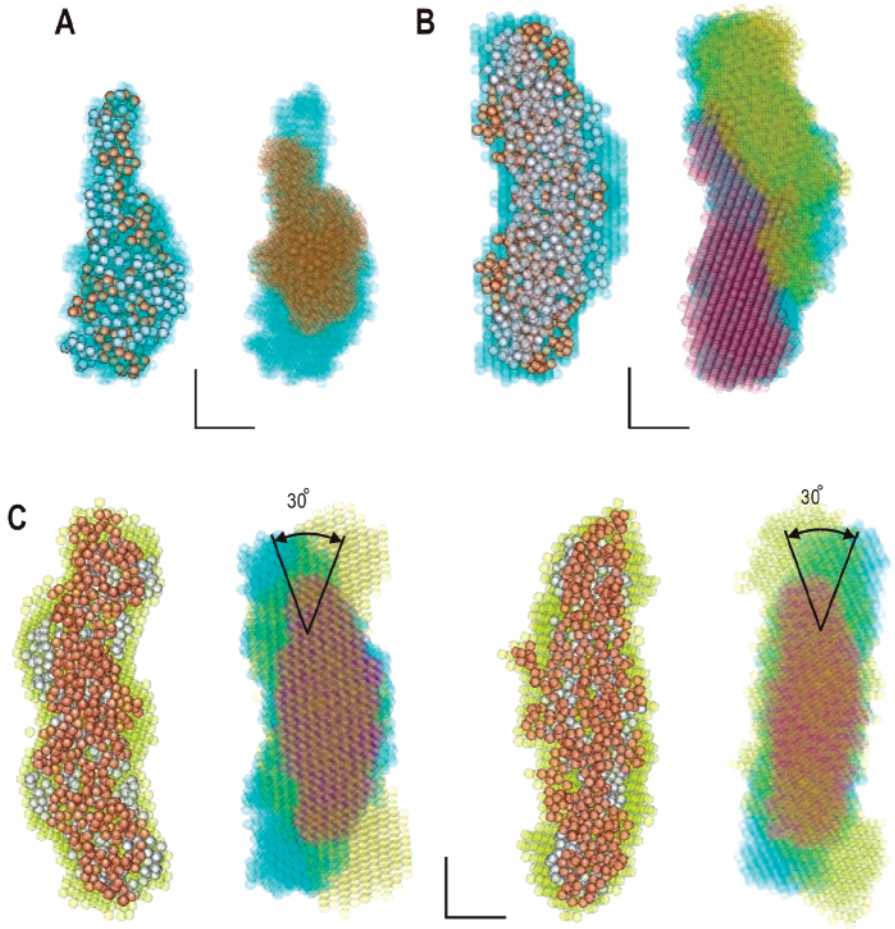

FIGURE 7: Molecular models of LOV2-linker fragments illustrated as in Figure 6. (A) Molecular models of the phot2 LOV2-linker fragment. In the right part, the molecular structure of phot2 LOV2 (brown spheres) is superimposed manually. (B) Molecular models of the phot1 LOV2-linker fragment in the dark. In the right part, the averaged model is approximated as an antiparallel association of two phot2 LOV2-linker models (yellow or purple). (C) Molecular models of the phot1 LOV2-linker fragment under blue-light irradiation. The first and third parts show the models viewed from two different directions. The second and fourth parts illustrate two possible superimpositions of the averaged model (yellow) onto that of the dark state (cyan) with phot1 LOV2 (purple) to maximally overlap their central portions. This figure was prepared with ASSA (*44*).

it is concluded that the light-induced SAXS changes of the wild-type phot1 LOV2-linker polypeptide are a result of formation of the cysteinyl adduct in the LOV2 core.

When a phot1 LOV2-linker polypeptide solution irradiated with blue light is kept in the dark, it takes ~4 h to recover the scattering profile observed before light irradiation (data not shown). In contrast, it takes ~26 s for the reversion from the cysteinyl adduct state to the dark state in the photoabsorption spectrum (Figure 1B). Because absorption measurement monitors the local structures around the FMN molecule, the results suggest that the interaction between the chromophore and its protein moiety does not directly reflect the changes in the overall structure. It is also suggested that the polypeptide undergoes gradual conformational relaxations predominantly through a thermal process.

DISCUSSION

Quaternary Structures of LOV Polypeptides. In the concentration range that has been examined, LOV1 polypeptides of both phot1 and phot2 exist as homodimers (Figures 3, 4, and 6 and Table 1), and their structural parameters and molecular structures are similar to each other (Figure 6). Because the polypeptide solutions used in the SAXS measurements are at much higher concentrations than those of intact phot *in vivo*, dimerization of the polypeptides during concentrating sample solutions cannot be excluded. However, these results suggest the dimeric association of the LOV1 polypeptides and possibly of full-length phot1 and phot2 at their LOV1 domains. Very recently, dimerization of oat phot1 at its LOV1 domain is proposed by using gel chromatography (*39*).

The LOV1 domain of either isoform has a minor role for activating the kinase domain as demonstrated in the rescue experiments of phot-deficient *A. thaliana* by phot with the combinations of the Cys-to-Ala mutant LOV1 and LOV2 domains (*28*). Therefore, the LOV1 domain of either isoform seems to act predominantly as a dimerization site and to have little interdomain interaction with the kinase domain. Homo- or heterodimerization of PAS domains is known to be profoundly important for cellular signal transduction (*40*−*42*). Because LOV domains are a subset of the PAS superfamily, the dimerization of LOV1 domains may also have functional importance. Thus, it is interesting to examine whether monomeric phot isoforms are active *in vivo*.

The quaternary structures of the LOV2 and LOV2-linker polypeptides are different between the isoforms. Although

it is difficult to deny completely the possibility of irreversible dimerization of the fragments in concentrated sample solutions at present, two other possible causes for the different quaternary structures should be noted. One is the differences in surface properties of the LOV2 core between the isoforms, because residues exposed to solvent in phot1 are replaced with those with the opposite electrostatic properties in phot2. Another is differences in the conformations of linker domains. The sequences of the 15 N-terminal residues in the linker domains (indicated with a box in Figure 1A) are quite different with respect to their electrostatic properties: phot2 contains only two negatively charged residues in this region and five in phot1. In preparing the phot2 LOV2-linker polypeptide, we detect a degradation product cleaved in the N-terminal region of the linker domain by endogenous proteinases of *E. coli*. The product is easily separated from the target polypeptide by gel chromatography. In contrast, the corresponding degradation product has not appeared in the preparation of phot1 LOV2-linker polypeptides. Thus, the N-terminal regions of the linker domains are expected to fold into distinct conformations between the isoforms and to influence the association of LOV2 domains.

Blue-Light-Induced Structural Changes in LOV Polypeptides. The phot1 LOV2-linker polypeptide exhibits blue-light-induced SAXS changes (Figures 2−5 and 7), while the phot1 LOV2 polypeptide does little in solution (Figures 2−6) and probably in the crystalline state as expected from phy3 LOV2 crystal structures (*26*). Thus, the SAXS changes in the phot1 LOV2-linker polypeptide are plausibly interpreted as a rearrangement of the linker domain relative to the LOV2 core and/or tertiary structural changes within the linker domain. When predicted models of phot1 LOV2-linker polypeptides are compared in the dark and under light irradiation, there are two ways to superimpose the models for overlapping maximally their middle portions plausibly assigned as LOV2 cores (Figure 7C). In either way, the edge portions seem to rotate ∼30° relative to the middle. Recently, a NMR study on an oat phot1-LOV2 polypeptide has revealed light-induced changes in the interactions between the LOV2 core and helix J in its linker region (*29*). Although the magnitude of the light-induced structural changes is not reported, the light-induced chemical shift seems to correlate closely with the structural changes observed in the SAXS experiments presented here. The LOV2 domain is proposed to inhibit ATP binding of the kinase domain in the dark and to release the inhibition upon blue-light irradiation. In a PAS kinase, the N-terminal PAS domain works as a ligand-regulated molecular switch inducing the kinase activity (*43*). Thus, in an analogy, the linker domain may also work as a regulator or a molecular switch amplifying the light-induced structural changes in the LOV2 core to the kinase domain.

In contrast to phot1, the LOV2-linker polypeptide of phot2 exhibits very small SAXS changes under blue-light irradiation. This may be partly caused by the differences in the quaternary structures and/or in the conformations of the 15 N-terminal residues of the linker domains, which are distinct between the isoforms (Figure 1A). The differences in the magnitude of light-induced conformational changes between isoforms may correlate with the physiological roles of phot1 and phot2 at the molecular level. phot1 mainly controls the chloroplast accumulation movement over a wide range of fluence rates, whereas phot2 mediates the avoidance under a high fluence rate (*8*, *9*). As seen in multisubunit enzymes, dimerization or higher-order association of subunits sometimes provides benefits for extending the dynamic ranges of sensitivities to external stimuli.

However, attention should be paid to the large differences in the half-life time of the cysteinyl adduct state observed in absorption measurements (Figure 1B). Even under strong blue-light irradiation, the short lifetime of the phot2 LOV2-linker polypeptide may result in a higher population of the dark state, when conformational changes are tightly coupled with the electronic state of the FMN moiety. To examine further this point, structural studies of any mutated polypeptides exhibiting very slow decay of the cysteinyl adduct state should be pursued in the future.

ACKNOWLEDGMENT

We thank Dr. K. Inoue and Ms. K. Miura of SPring-8/JASRI for their kind help in tuning the instruments and the modification of BL40B2 to measure SAXS under the dark conditions and Dr. H. Imai and Prof. Y. Shichida of the Graduate School of Science (Kyoto University, Kyoto, Japan) for their help in the spectroscopic measurements of the LOV2-containing polypeptides.

REFERENCES

1. Quail, P. H. (2002) Photosensory perception and signaling in plant cells: new paradigms? *Curr. Opin. Cell Biol. 140*, 180−188.
2. Quail, P. H. (2002) Phytochrome photosensory signaling networks, *Nat. Rev. Mol. Cell Biol. 3*, 85−93.
3. Cashmore, A. R. (2003) Cryptochromes: enabling plants and animals to determine circadian time, *Cell 114*, 537−543.
4. Briggs, W. R., Beck, C., Cashmore, A. R., Christie, J. M., Hughes, J., Jarillo, J. A., Kagawa, T., Kanegae, H., Liscum, E., Nagatani, A., Okada, K., Salomon, M., Rüdiger, W., Sakai, T., Takano, M., Wada, M., and Watson, J. C. (2001) The phototropin family of photoreceptors, *Plant Cell 13*, 993−997.
5. Briggs, W. R., and Christie, J. M. (2002) Phototropins 1 and 2: versatile plant blue-light receptors, *Trends Plant Sci. 7*, 204−210.
6. Christie, J. M., Reymond, P., Powell, G. K., Bernasconi, P., Raibekas, A., Liscum, E., and Briggs, W. R. (1998) *Arabidopsis* NPH1: a flavoprotein with the properties of a photoreceptor for phototropism, *Science 282*, 1698−1701.
7. Kagawa, T., Sakai, T., Suetsugu, N., Oikawa, K., Ishiguro, S., Kato, T., Tabata, S., Okada, K., and Wada, M. (2001) *Arabidopsis* NPL1: A phototropin homolog controlling the chloroplast high-light avoidance response, *Science 291*, 2138−2141.
8. Sakai, T., Kagawa, T., Kasahara, M., Swartz, T., Christie, J. M., Briggs, W. R., Wada, M., and Okada, K. (2001) Photochemical properties of the flavin mononucleotide-binding domains of the phototropins from *Arabidopsis*, rice, and *Chlamydomonas reinhardtii*, *Proc. Natl. Acad. Sci. U.S.A. 98*, 6969−6974.
9. Jarillo, G. A., Gabrys, H., Capel, J., Alonso, J. M., Ecker, J. R., and Cashmore, A. R. (2001) Phototropin-related NPL1 controls chloroplast relocation induced by blue light, *Nature 410*, 952−954.
10. Kinoshita, T., Doi, M., Suetsugu, N., Kagawa, T., Wada, M., and Shimazaki, K. (2001) Phot1 and phot2 mediate blue light regulation of stomatal opening, *Nature 414*, 656−660.
11. Liscum, E., and Briggs, W. R. (1995) Mutations in the NPH1 locus of *Arabidopsis* disrupt the perception of phototropic stimuli, *Plant Cell 7*, 473−485.
12. Stowe-Evans, E. L., Luesse, D. R., and Liscum, E. (2002) The enhancement of phototropin-induced phototropic curvature in *Arabidopsis* occurs via a photoreversible phytochrome A-dependent modulation of auxin responsiveness, *Plant Physiol. 2001*, 826−834.
13. Harada, A., Sakai, T., and Okada, K. (2003) Phot1 and phot2 mediate blue light-induced transient increases in cytosolic Ca^{2+} differently in *Arabidopsis* leaves, *Proc. Natl. Acad. Sci. U.S.A. 100*, 8583−8588.

14. Baum, G., Long, J. C., Jenkins, G. I., and Trewavas, A. J. (1999) Stimulation of the blue light phototropic receptor NPH1 causes a transient increase in cytosolic Ca^{2+}, *Proc. Natl. Acad. Sci. U.S.A. 96*, 13554−13559.
15. Kinoshita, T., and Shimazaki, K (1999) Blue light activates the plasma membrane $H^{(+)}$-ATPase by phosphorylation of the C-terminus in stomatal guard cells, *EMBO J. 18*, 5548−5558.
16. Christie, J. M., Salomon, M., Nozue, K., Wada, M., and Briggs, W. R. (1999) LOV (light, oxygen, or voltage) domains of the blue-light photoreceptor phototropin (nph1): binding sites for the chromophore flavin mononucleotide, *Proc. Natl. Acad. Sci. U.S.A. 96*, 8779−8783.
17. Cheng, P., He, Q., Yang, Y., Wang, L., and Liu, Y. (2003) Functional conservation of light, oxygen, or voltage domains in light sensing, *Proc. Natl. Acad. Sci. U.S.A. 100*, 5938−5943.
18. Taylor, B. L., and Zhulin, I. B. (1999) PAS domains: internal sensors of oxygen, redox potential and light, *Microbiol. Mol. Biol. Rev. 63*, 479−506.
19. Miller, S. M., Massy, V., Ballou, D., Williams, C. H., Jr., Distefano, M. D., Moore, M. J., and Walsh, C. T. (1990) Use of a site-directed triple mutant to trap intermediates: demonstration that the flavin C(4a)-thiol adduct and reduced flavin are kinetically competent intermediates in mercuric ion reductase, *Biochemistry 29*, 2831−2841.
20. Salomon, M., Christie, J. M., Kneib, E., Lempert, U., and Briggs, W. R. (2000) Photochemical and mutational analysis of the FMN-binding domains of the plant blue light receptor, phototropin, *Biochemistry 39*, 9401−9410.
21. Swartz, T. E., Corchnoy, S. B., Christie, J. M., Lewis, J. W., Szundi, I., Briggs, W. R., and Bogomolni, R. A. (2001) The photocycle of a flavin-binding domain of the blue light photoreceptor phototropin, *J. Biol. Chem. 276*, 36493−36500.
22. Iwata, T., Tokutomi, S., and Kandori, H. (2002) Photoreaction of the cysteine S−H group in the LOV2 domain of *Adiantum* phytochrome3, *J. Am. Chem. Soc. 124*, 11840−11841.
23. Iwata, T., Nozaki, D., Tokutomi, S., Kagawa, T., Wada, M., and Kandori, H. (2003) Light-induced structural changes in the LOV2 domain of *Adiantum* phytochrome3 studied by low-temperature FTIR and UV−visible spectroscopy, *Biochemistry 42*, 8183−8191.
24. Fedorov, R., Schlichting, I., Hartmann, E., Domratcheva, T., Fuhrmann, M., and Hegemann, P. (2003) Crystal structures and molecular mechanism of a light-induced signaling switch: The Phot-LOV1 domain from *Chlamydomonas reinhardtii*, *Biophys. J. 84*, 2474−2482.
25. Crosson, S., and Moffat, K. (2001) Structure of a flavin-binding plant photoreceptor domain: Insights into ligand-mediated signal transduction, *Proc. Natl. Acad. Sci. U.S.A. 98*, 2995−3000.
26. Crosson, S., and Moffat, K. (2002) Photoexcited structure of a plant photoreceptor domain reveals a light-driven molecular switch, *Plant Cell 14*, 1067−1075.
27. Crosson, S., Rajagopal, S., and Moffat, K. (2003) The LOV domain family: Photoresponsive signaling modules coupled to diverse output domains, *Biochemistry 42*, 2−10.
28. Christie, J. M., Swartz, T. E., Bogomolni, R. A., and Briggs, W. R. (2002) Phototropin LOV domains exhibit distinct roles in regulating photoreceptor function, *Plant J. 32*, 205−219.
29. Harper, S. M., Neil, L. C., and Gardner, K. H. (2003) Structural basis of a phototropin light switch, *Science 301*, 1541−1544.
30. Feigin, L. A., and Svergun, D. I. (1987) *Structure Analysis by Small-angle X-ray and Neutron Scattering*, Plenum Press, New York.
31. Fujisawa, T., Inoko, Y., and Yagi, N. (1999) The use of a Hamamatsu X-ray image intensifier with a cooled CCD as a solution X-ray scattering detector, *J. Synchrotron Radiat. 6*, 1106−1114.
32. Giunier, A., and Fournet, G. (1955) *Small-Angle Scattering of X-rays*, John Wiley, New York.
33. Svergun, D. I. (1992) Determination of the regularization parameter in indirect-transform methods using perceptual criteria, *J. Appl. Crystallogr. 25*, 495−503.
34. Fukuhara, N., Fernandez, E., Ebert, J., Conti, E., and Svergun, D. (2004) Conformational variability of nucleo-cytoplasmic transport factor, *J. Biol. Chem. 279*, 2176−2181.
35. Svergun, D. I. (1999) Restoring low resolution structure of biological macromolecules from solution scattering using simulated annealing, *Biophys. J. 76*, 2879−2886.
36. Svergun, D. I., Petoukhov, M. V., and Koch, M. H. J. (2001) Determination of domain structure of proteins from X-ray solution scattering, *Biophys. J. 80*, 2946−2953.
37. Kozin, M. B., and Svergun, D. I. (2001) Automated matching of high- and low-resolution structural models, *J. Appl. Crystallogr. 34*, 33−41.
38. Kasahara, M., Swartz, T. E., Olney, S. M., Onodera, A., Mochizuki, N., Fukuzawa, H., Asamizu, E., Tabata, S., Kanegae, H., Takano, M., Christie, J. M., Nagatani, A., and Briggs, W. R. (2002) Photochemical properties of the flavin mononucleotide-binding domains of the phototropins from *Arabidopsis*, rice, and *Chlamydomonas reinhardtii*, *Plant Physiol. 129*, 762−773.
39. Salomon, M., Lempert, U., and Rüdiger, W. (2004) Dimerization of the plant photoreceptor phototropin is probably mediated by the LOV domain, *FEBS Lett. 572*, 8−10.
40. Lindebro, M. C., Poellinger, L., and Whitelaw, M. L. (1995) Protein−protein interaction via PAS domains: role of the PAS domain in positive and negative regulation of the bHLH/PAS dioxin receptor-Arnt, *EMBO J. 14*, 3528−3539.
41. Sogawa, K., Nakano, R., Kobayashi, A., Kikuchi, Y., Ohe, N., Matsushita, N., and Fujii-Kuriyama, Y. (1995) Possible function of Ah receptor nuclear translocator (Arnt) homodimer in transcriptional regulation, *Proc. Natl. Acad. Sci. U.S.A. 92*, 1936−1940.
42. Ballario, P., Talora, C., Galli, D., Linden, H., and Macino, G. (1998) Roles in dimerization and blue light photoresponse of the PAS and LOV domains of *Neurospora crassa* white collar proteins, *Mol. Microbiol. 29*, 719−729.
43. Amezcua, A. A., Harper, S. M., Rutter, J., and Gardner, K. H. (2002) Structure and interactions of PAS kinase N-terminal PAS domain: Model for intramolecular kinase regulation, *Structure 10*, 1349−1361.
44. Kozin, M. B., and Svergun, D. I. (1997) ASSA: A program for three-dimensional rendering in solution scattering from biopolymers, *J. Appl. Crystallogr. 34*, 33−41.

BI0485530